

Two RHIC puzzles: Early thermalization and the HBT problem

Ulrich Heinz and Peter F. Kolb

Physics Department, The Ohio State University, Columbus, OH 43210, USA

Abstract. Hadron spectra from the first year RHIC run are shown to be excellently reproduced by hydrodynamic calculations. We argue that in particular the elliptic flow data provide strong evidence for early thermalization at RHIC, at energy densities well above deconfinement, but that the phenomenologically extracted short thermalization time scale of less than $1 \text{ fm}/c$ provides a serious challenge for theory. The HBT radii from the hydrodynamic calculations agree only qualitatively with the data, showing significant quantitative discrepancies. It is argued that this points to a still incomplete understanding of the freeze-out process at RHIC.

Keywords: Relativistic heavy-ion collisions, hydrodynamics, thermalization, two-particle correlations

PACS: 25.75.-q, 25.75.Ld, 25.75.Gz, 24.10.Nz

1. Elliptic flow as an early QGP signature

The quark-gluon plasma (QGP) is a thermalized system and, as such, has thermal pressure. If the QGP is created in a heavy-ion collision, this pressure acts against the surrounding vacuum and causes a rapid collective expansion (“flow”) of the reaction zone, the “Little Bang”. In non-central collisions the initial overlap region of the two nuclei is elliptically deformed in the transverse plane, resulting in anisotropic pressure gradients. These cause a more rapid expansion into the reaction plane than perpendicular to it, resulting in an anisotropy of the final transverse momentum distribution called *elliptic flow* [1]. Elliptic flow is quantified by the second harmonic coefficient $v_2(y, p_\perp; b)$ of a Fourier expansion in ϕ_p of the measured hadron spectrum $dN/(dy p_\perp dp_\perp d\phi_p)$ [2]. At midrapidity in collisions between equal-mass nuclei it is the lowest-order non-zero Fourier coefficient.

Since individual nucleon-nucleon collisions produce azimuthally symmetric spectra, any final state momentum anisotropies must be generated dynamically during the nuclear reaction. A non-zero value for the elliptic flow is thus an unambiguous sign for reinteractions among the produced particles, and its magnitude characterizes their strength. Microscopic transport calculations [3, 4] show a monotonic dependence of v_2 on the opacity (density times scattering cross section) of the produced matter which is inversely related to its thermalization time. Elliptic flow also requires the existence of an initial spatial anisotropy of the reaction zone, by colliding either deformed nuclei at $b=0$ or spherical

nuclei at $b \neq 0$. The transport calculations strongly suggest that, for a given initial spatial anisotropy ϵ_x , the maximum momentum-space response v_2 is obtained in the *hydrodynamic limit* which assumes a thermalization time which is much shorter than any macroscopic time scale in the system. Any significant delay of thermalization allows the initial spatial deformation to decay without concurrent build-up of momentum anisotropies, thereby reducing the finally observed elliptic flow signal [5].

This specific sensitivity of the elliptic flow to rescattering and pressure build-up in the early collision stages [6, 7] (before the spatial deformation and the resulting anisotropies of the pressure gradients have disappeared [5]) puts v_2 on the list of “early signatures” of the collision dynamics. In contrast to other early probes (which use rare signals such as hard photons and dileptons, heavy quarkonia and jets), v_2 can be extracted from the bulk of the measured hadrons which are very abundant and thus easily accessible. In fact, the elliptic flow measurement in Au+Au collisions at $\sqrt{s} = 130\text{A GeV}$ [8] became the *second* publication of RHIC data and appeared within days of the end of the first RHIC run.

We present hydrodynamic results for hadronic spectra and elliptic flow at RHIC energies. We show that the hydrodynamic approach provides an excellent quantitative description of the bulk of the data and fails only for very peripheral Au+Au collisions and/or at high $p_\perp > 1.5\text{--}2\text{ GeV}/c$. That the hydrodynamic approach fails for small initial overlap regions or large hadron transverse momenta is not unexpected. What is surprising is that the hydrodynamic approach *does* work for such a wide range of impact parameters and p_\perp and quantitatively reproduces the momenta of more than 99% of the particles: below $p_\perp = 1.5\text{ GeV}/c$ the elliptic flow data [8, 9, 10] actually exhaust the hydrodynamically predicted [5, 11, 12, 13, 14] upper limit. The significance of this agreement can hardly be overstressed, and it poses significant challenges for microscopic descriptions of the early collision dynamics. How the system is able to thermalize so fast is the first RHIC puzzle which we point out.

The second puzzle arises from two-particle correlation measurements (HBT interferometry) [15, 16] which constrain the freeze-out distribution in space-time. The same hydrodynamic model which provides an almost perfect description of the momentum-space structure of the emitting source (spectra and elliptic flow) predicts a space-time distribution at freeze-out which, when translated into HBT radii, does not agree very well with the data. We argue in Sec. 3 that this points to a problem with our understanding of the late freeze-out stage of the collision.

2. Radial and elliptic flow from hydrodynamics

The natural language for describing collective flow phenomena is hydrodynamics. In the ideal fluid (non-viscous) limit used by us, this approach assumes that the microscopic momentum distribution is thermal at every point in space and time. This does not require chemical equilibrium – chemically non-equilibrated situations can be treated by solving separate and coupled conservation equations for the particle currents of individual particle species. The assumption of local thermal equilibrium is an external input, and hydrodynamics offers no insights about the equilibration mechanisms. It is clearly invalid during

the initial particle production and early rescattering stage, and it again breaks down towards the end when the matter has become so dilute that rescattering ceases and the hadrons “freeze out”. The hydrodynamic approach thus requires a set of *initial conditions* for the hydrodynamic variables at the earliest time at which the assumption of local thermal equilibrium is applicable, and a “*freeze-out prescription*” at the end. For the latter we use the Cooper-Frye algorithm [17] which implements an idealized sudden transition from perfect local thermal equilibrium to free-streaming. A better algorithm [18, 12] switches from a hydrodynamic description to a microscopic hadron cascade at or shortly after the quark-hadron transition, before the matter becomes too dilute, and lets the cascade handle the freeze-out kinetics. The resulting flow patterns [12] from such an improved freeze-out algorithm don’t differ much from our simpler Cooper-Frye based approach.

The main advantage of the microscopic freeze-out algorithm [18, 12] is that it also correctly reproduces the final chemical composition of the fireball, since the particle abundances already freeze out at hadronization, due to a lack of particle-number changing inelastic rescattering processes in the hadronic phase [19]. Our version of the hydrodynamic approach uses an equation of state which assumes local chemical equilibrium all the way down to kinetic freeze-out at $T_f \approx 125$ MeV and thus is unable to reproduce the correct hadron yield ratios. We therefore adjust the normalization of the momentum spectra for the rarer particle species (kaons, protons, antiprotons) in central collisions by hand to reproduce the chemical equilibrium ratios at a chemical freeze-out temperature $T_{\text{chem}} = 165$ MeV. The absolute normalization of the pion spectra is adjusted through the initial energy density in central collisions; for non-central collisions no new parameters enter since the centrality dependence of the initial conditions is completely controlled by the collision geometry.

To simplify the numerical task of solving the hydrodynamic equations we analytically impose boost invariant longitudinal expansion [20, 1]. This doesn’t give up any essential physics as long as we focus on the transverse expansion dynamics near midrapidity (the region which most RHIC experiments cover best). The hydrodynamic expansion starts at time τ_{eq} which we fixed by a fit to hadron spectra from the SPS and then extrapolated to RHIC initial conditions (for details see [5, 13]). For each impact parameter the initial energy density profile in the transverse plane is calculated from a Glauber parametrization using realistic nuclear thickness functions [5, 21]. The measured centrality dependence of the charged particle rapidity density at midrapidity, $(dN_{\text{ch}}/dy)(y=0)$, selects certain allowed combinations of “hard” and “soft” mechanisms for the initial particle production [21]. We here present results for initial conditions at $\tau_{\text{eq}} = 0.6$ fm/c calculated from a mixture of 25% “hard” (binary collision) and 75% “soft” (wounded nucleon) contributions [21] to the initial *entropy density* (or parton density), with a maximal entropy density $s_{\text{max}} = 85/\text{fm}^3$ at the fireball center in central collisions (corresponding to a maximal energy density $e_{\text{max}} = 21.4 \text{ GeV/fm}^3$ and a maximal temperature $T_{\text{max}} = 328$ MeV). At the standard time $\tau = 1$ fm/c used in Bjorken’s formula [20] for estimating the energy density from the measured multiplicity density, this corresponds to an average energy density $\langle e \rangle(1 \text{ fm/c}) = 5.4 \text{ GeV/fm}^3$ which is about 70% higher than the value reported from $158A$ GeV Pb+Pb collisions at the SPS. (Note that $\langle e \rangle$ at $\tau_{\text{eq}} = 0.6$ fm/c is nearly twice as large!) The corresponding profiles for peripheral collisions are then given by the Glauber model [5, 21]. Kinetic freeze-out was forced at $T_f = 130$ MeV, independent of centrality.

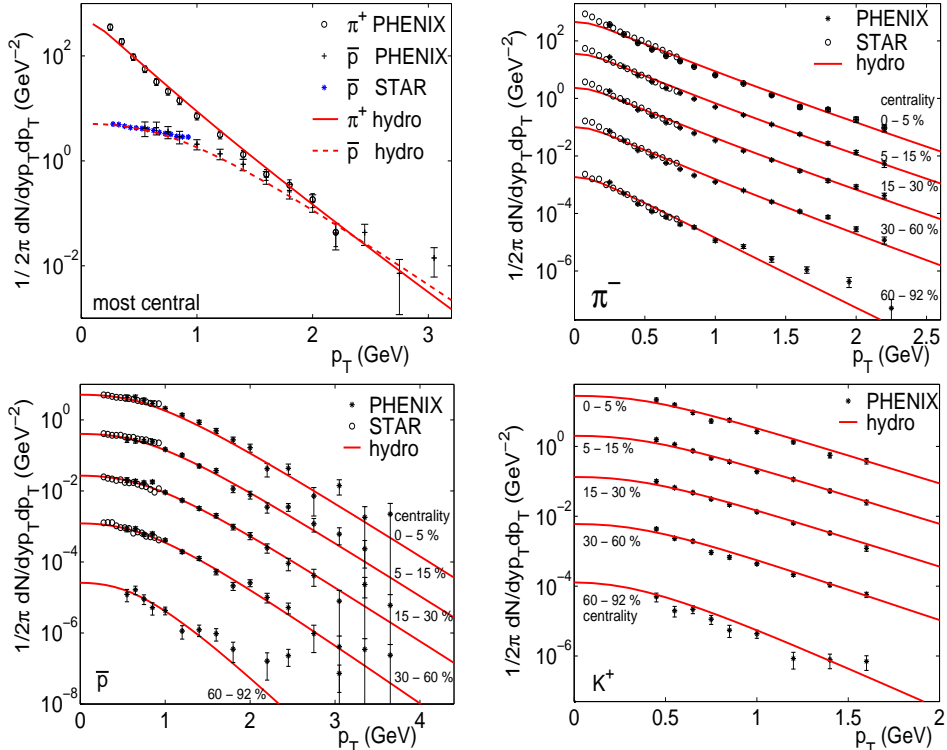


Fig. 1. Charged pion, antiproton and positive kaon spectra from central (upper left panel) and semi-central to peripheral (other three panels) Au+Au collisions at $\sqrt{s}=130A$ GeV. The data were taken by the PHENIX [24] and STAR [25] collaborations (the STAR data have slightly different centralities than the indicated values from PHENIX). The curves show hydrodynamical calculations (see text).

Fig. 1 shows the (absolutely normalized) single particle p_{\perp} -spectra for charged pions, antiprotons and kaons measured in Au+Au collisions at RHIC together with the hydrodynamical results. The latter were normalized in central collisions as described above, but their centrality dependence and shapes are then completely fixed by the model. The agreement with the data is impressive; for antiprotons the data go out to $p_{\perp} \leq 3$ GeV/c, and the hydrodynamic model still works within errors! Only for very peripheral collisions (impact parameter $b > 10$ fm) the data show a significant excess of high- p_{\perp} particles at $p_{\perp} > 1.5$ GeV/c. Teaney *et al.* [12] showed that this excellent agreement *requires* a phase transition (soft region) in the equation of state; without the transition, the agreement is lost, especially when the constraints from SPS data and from the elliptic flow measurements below are taken into account.

In the hydrodynamic picture the fact that antiprotons become more abundant than pions for $p_{\perp} > 2$ GeV/c (upper left panel of Fig. 1) is not surprising at all: it is a simple consequence of the strong radial flow at RHIC. For a hydrodynamically expanding thermalized fireball, at relativistic transverse momenta $p_{\perp} \gg m_0$ all hadron spectra have the same

shape [26], and at fixed $m_{\perp} \gg m_0$ their relative normalization is given by $(g_i \lambda_i)/(g_j \lambda_j)$ (where $g_{i,j}$ is the spin-isospin degeneracy factor and $\lambda_{i,j} = e^{\mu_{i,j}/T}$ is the fugacity of hadron species i,j). At RHIC the baryon chemical potential at chemical freeze-out is small, $\mu_B/T_{\text{chem}} \approx 0.26$ [27], and $\mu_{\pi} = 0$; the \bar{p}/π^- ratio at fixed and sufficiently large m_{\perp} is thus predicted to be larger than 1: $(\bar{p}/\pi^-)_{m_{\perp}} = 2 \exp[-(\mu_B + \mu_{\pi})/T_{\text{chem}}] \approx 1.5$ (where the factor 2 arises from the spin degeneracy of the \bar{p}).

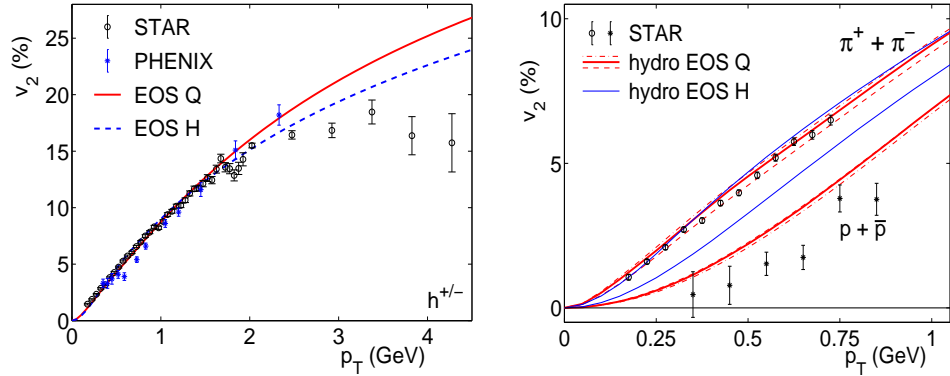


Fig. 2. The elliptic flow coefficient $v_2(p_{\perp})$ for all charged particles (left) and for identified pions and protons (right) from $130A$ GeV minimum bias Au+Au collisions [8, 9, 28, 29]. The curves are hydrodynamic calculations corresponding to equations of state with (Q) and without (H) a phase transition and (in the right panel) three different freeze-out temperatures ($T_f = 128$ MeV (dash-dotted), 130 MeV (solid) and 134 MeV (dashed)).

Figure 2 compares the differential elliptic flow $v_2(p_{\perp})$ from minimum bias Au+Au collisions at RHIC [8, 28, 29] with hydrodynamic calculations. For transverse momenta $p_{\perp} < 2$ GeV/c the data are seen to exhaust the upper limit for v_2 obtained from the hydrodynamic calculations. Only for hadrons with $p_{\perp} > 2$ GeV/c (i.e. fewer than 1% of all) v_2 stays below the hydrodynamic upper limit, indicating incomplete thermalization of high- p_{\perp} particles. The data also show the hydrodynamically predicted mass-dependence of v_2 [14] (right panel). Similar conclusions can be drawn from a plot of the p_{\perp} -integrated elliptic flow vs. centrality [13, 21]: only for large impact parameters $b > 7$ fm the measured v_2 remains significantly below the hydrodynamic prediction, presumably indicating a lack of early thermalization when the initial overlap region becomes too small.

The excellent agreement with hydrodynamics becomes even more impressive after you begin to realize how easily it is destroyed: As stressed in Sec. 1, it requires the build-up of momentum anisotropies during the very early collision stages when the spatial anisotropy of the reaction zone is still appreciable, causing significant anisotropies of the pressure gradients. A delay in thermalization by more than about 1 fm/c (2 fm/c) dilutes the spatial anisotropy and the hydrodynamically predicted elliptic flow coefficient by 10% (25%) [5] which is more than is allowed by the data. Parton cascade simulations with standard HIJING input generate almost no elliptic flow and require an artificial increase of the opacity of the partonic matter by a factor 80 to reproduce the RHIC data [4]. Hadronic cascades of the RQMD and URQMD type (in which the high-density initial state is parametrized

by non-interacting, pressureless QCD strings) predict [30] too little elliptic flow and a decrease of v_2 from SPS to RHIC, contrary to the data. One can get close to the data by forcing the strings to “melt” into partons which then rescatter with large cross sections [31]. What causes these large cross sections is still a mystery.

The elliptic flow is self-quenching [6]: it makes the reaction zone grow faster along its initially short direction and thus eventually eliminates its own cause. As the spatial deformation of the fireball goes to zero, the elliptic flow saturates [5]. The saturation time scale times c is of the order of the transverse size of the initial overlap region (at lower energies it is a bit longer, see Figs. 7, 9 in [5]). At RHIC energies and above, the time it takes the collision zone to dilute from the high initial energy density to the critical value for hadronization is equal to or longer than this saturation time: most or all of the elliptic flow is generated before any hadrons even appear! It thus seems that the only possible conclusion from the successful hydrodynamic description of the observed radial and elliptic flow patterns is that the thermal pressure driving the elliptic flow is partonic pressure, and that the early stage of the collision must have been a thermalized quark-gluon plasma.

3. The RHIC HBT puzzle

Hydrodynamics not only predicts the momenta of the emitted hadrons, but also the spatial structure of the hadron emitting source at freeze-out. Bose-Einstein (a.k.a. Hanbury Brown-Twiss (HBT)) two-particle intensity interferometry allows to access the r.m.s. widths of the space-time distribution of hadrons with a given momentum p [32]. One of the interesting questions one can try to address with this tool is whether at RHIC the reaction zone flips the sign of its spatial deformation between initial impact and final freeze-out, as expected at very high collision energy [5]. The answer to this question turns out to be non-trivial, on two different levels: first, hydrodynamics, at least with the presently implemented initial conditions and freeze-out algorithm, fails to reproduce even for central Au+Au collisions the measured HBT radii extracted from two-pion correlations [15, 16]. We’ll show how and explain why. Second, for expanding systems the HBT radii don’t measure the entire freeze-out region, but only the effective emission regions (“regions of homogeneity”) for particles of given momentum [32]. For non-central collisions, due to the anisotropic transverse flow these can, at least in principle, have a different spatial deformation than the entire (momentum-integrated) freeze-out region, giving rise to a different behaviour of the HBT radii observed at different angles relative to the reaction plane than perhaps naively expected [33].

Fig. 3 shows the HBT radii R_{side} , R_{out} , and R_{long} for central Au+Au collisions at $\sqrt{s}=130A$ GeV [15, 34] compared with hydrodynamic results. The theoretical results only account for directly emitted pions; resonance decay pions would add an exponential tail to the emission time distribution and could cause a slight increase in the emission duration, without affecting much the spatial width of the emission region [35]. The solid lines correspond to initial conditions and freeze-out parameters as used for the successful description of the momentum distributions in the previous section; clearly, R_{side} comes out

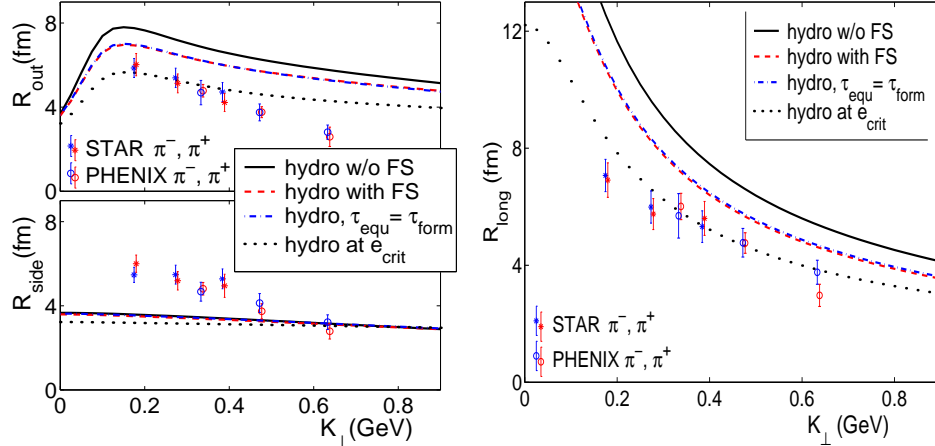


Fig. 3. HBT radii from a hydrodynamic source compared to RHIC data [15, 34]. The solid lines show hydrodynamic results with standard initialization and freeze-out (see text). The dotted lines assume freeze-out directly after hadronization at $e_{\text{dec}} = e_{\text{crit}}$. The other lines correspond to modified initial conditions as described in the text.

too small whereas R_{out} and R_{long} are both too large in the model. The problem of R_{side} from hydrodynamics being too small is well-known from the SPS [36]; presumably it is mostly due to the sharp Cooper-Frye freeze-out and seems to be at least partially resolved if the freeze-out kinetics is handled microscopically within a hadronic cascade [37]. The latter gives a more “fuzzy” spatial freeze-out distribution with larger r.m.s. width in the sideward direction; it is not so clear that it also resolves the problem with the K_{\perp} -dependence of R_{side} which is much stronger in the data than in the model.

On the other hand, “fuzzy” freeze-out [37] and the inclusion of resonance decay contributions [35] only exacerbate the problems with R_{long} and R_{out} . In high energy heavy-ion collisions the longitudinal HBT radius is controlled by the expansion dynamics via the longitudinal velocity gradient at freeze-out [32]. For a boost invariant longitudinal flow profile this gradient decreases with time as $1/\tau$, leading to rather weak gradients (and correspondingly large values for R_{long}) at the typical hydrodynamic freeze-out time of $\sim 15 \text{ fm}/c$. To reduce R_{long} , either freeze-out must happen significantly earlier, or the expansion of the source must strongly violate longitudinal boost-invariance even close to mid-rapidity, somehow allowing for significantly stronger longitudinal flow velocity gradients at late times than predicted by the Bjorken profile $v_L = z/t$.

Noting that decoupling is driven by the strong radial flow developing during the expansion stage [38], we have tried to force the system to decouple earlier by initiating the transverse flow even before τ_{eq} . Even if the system is not yet locally thermalized, it will start to develop some transverse collective dynamics, albeit perhaps not as quickly as in a hydrodynamic approach. We have tested two extreme assumptions about the transverse expansion prior to thermalization [39]: in one simulation, shown as the dot-dashed curve in Fig. 3, we started the hydrodynamic evolution directly at the parton formation time (for which we took the somewhat arbitrary value $\tau_{\text{form}} = 0.2 \text{ fm}/c$). In another limit (dashed lines in Fig. 3), we allowed the partons to stream freely from time τ_{form} to τ_{eq} and matched

at τ_{eq} the first row of the energy momentum tensor to an ideal fluid form, thereby extracting an initial transverse flow profile at τ_{eq} . In both cases the resulting transverse flow “seed” at $\tau_{\text{eq}}=0.6 \text{ fm}/c$ caused the system to expand more rapidly and farther out into the transverse direction, freezing out 10-20% earlier. Fig. 3 shows that this helps with both R_{long} and R_{out} , but not as much as required by the data.

To get close to the data, we would need to postulate freeze-out directly at the hadronization point (dotted lines in Fig. 3). This radical and entirely unmotivated assumption almost removes the discrepancy with R_{long} and with the average magnitude of R_{out} , but it is still unable to reproduce the measured strong K_{\perp} -dependence of R_{out} and R_{side} , and it still yields much too small values for R_{side} at low K_{\perp} . Correspondingly, the ratio $R_{\text{out}}/R_{\text{side}}$ (which is ≈ 1 in the data) is still significantly overpredicted by the model (although much less so than by earlier hydrodynamic predictions [40] when constraints from RHIC momentum spectra were not yet available).

The problem with the small R_{side} cannot be fixed by pre-equilibrium transverse flow, either: even though the system then expands to larger values of r , R_{side} remains essentially unchanged (dashed and dash-dotted lines in Fig. 3). The homogeneity region simply moves farther out without increasing in size. We don’t see a way to move closer to the data by further modifying the initial conditions, and even the alterations we made to obtain Fig. 3 may turn out to be excluded by the singles spectra and the elliptic flow data (which we haven’t tested yet). We therefore believe that a resolution to the HBT puzzle must lie in the handling of the freeze-out process (although we don’t yet know how).

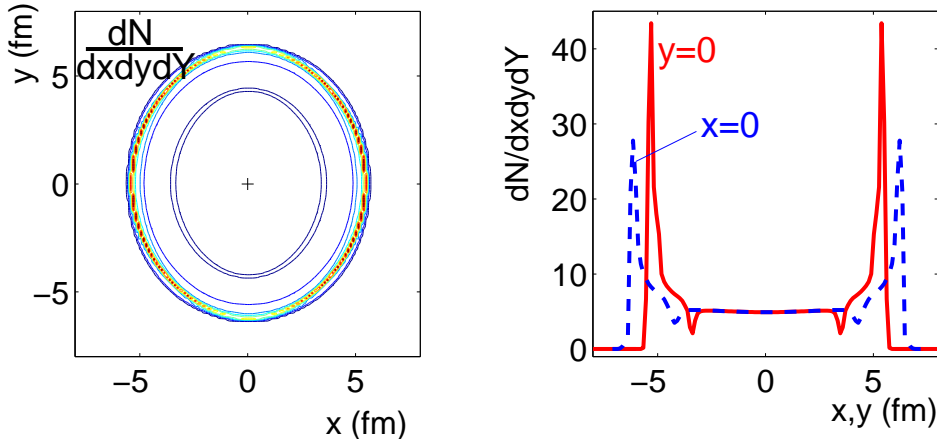


Fig. 4. The K_{\perp} -integrated emission function from hydrodynamics, for directly emitted pions with rapidity $Y = 0$ from semicentral Au+Au collisions ($b=7 \text{ fm}$). The emission function is integrated over time and longitudinal coordinate z . The left panel shows contours of constant particle density in the transverse plane, the right panel presents cuts through this distribution along the x and y axes, showing that particle emission is strongly concentrated at the surface, especially for emission into the reaction plane ($y=0$).

Let us further analyze the relationship between R_{out} and R_{side} . The formula [32]

$$R_{\text{out}}^2 - R_{\text{side}}^2 = \langle (x_{\text{out}} - \bar{x}_{\text{out}})^2 - (x_{\text{side}} - \bar{x}_{\text{side}})^2 \rangle + \beta_{\perp}^2 \langle (t - \bar{t})^2 \rangle - 2\beta_{\perp} \langle (x_{\text{out}} - \bar{x}_{\text{out}})(t - \bar{t}) \rangle \quad (1)$$

shows that their difference is controlled by three contributions which can partially compensate each other. There is always a positive contribution from the emission duration $(\delta t)^2 \equiv \langle (t - \bar{t})^2 \rangle$; for systems with longitudinal boost-invariance freeze-out happens at constant longitudinal proper time $\tau = \tau_f$, and late freeze-out, which leads to a large longitudinal homogeneity region R_{long} , thus implies contributions from a wide region along this $\tau = \tau_f$ hyperbola, leading to a large variance δt . To reduce δt we should therefore again freeze out earlier. In hydrodynamics with Cooper-Frye freeze-out [17], the term $-2\beta_\perp \langle (x_{\text{out}} - \bar{x}_{\text{out}})(t - \bar{t}) \rangle$ is also positive, since freeze-out happens from the outside inward, causing a negative $x_{\text{out}} - t$ correlation. These two positive contributions to $R_{\text{out}}^2 - R_{\text{side}}^2$ are partially cancelled by a negative geometric contribution $(\delta x_{\text{out}})^2 - (\delta x_{\text{side}})^2$: according to Figures 4 and 5 hydrodynamics predicts that pion emission is strongly surface dominated, especially for pions with non-zero transverse momentum K_\perp , whose emission regions are tightly squeezed towards the edge of the fireball where the radial flow is strongest. This results in an ‘‘opaque source’’, characterized by a smaller outward than sideward variance $(\delta x_{\text{out}})^2 < (\delta x_{\text{side}})^2$ [41]. The opacity of the hydrodynamic source is stronger at RHIC than SPS energies, but not strong enough to compensate for the two positive contributions in Eq. (1); this is the reason why we fail to reproduce the measured relation $R_{\text{out}} \approx R_{\text{side}}$. Of course, things would be easier if the $x_{\text{out}} - t$ correlation were positive (i.e. pions at larger radial distances were emitted later), but we don’t see a good reason why this should be so.

Let us close with a quick preview of results for the HBT radii for non-central collisions, in particular their dependence on the angle Φ of the transverse pair momentum \vec{K}_\perp relative to the reaction plane. Fig. 6 shows our hydrodynamic results for R_{side}^2 , R_{out}^2 , R_{os}^2 , and R_{long}^2 for $b = 7$ fm Au+Au collisions at $\sqrt{s} = 130$ A GeV, plotted as functions of Φ for a number of different values of $K_\perp = |\vec{K}_\perp|$. (Note that ‘‘out’’ and ‘‘side’’ denote the directions parallel and perpendicular to \vec{K}_\perp in the transverse plane [32].) While R_{long}^2 is almost independent of Φ , the three other radius parameters show marked azimuthal dependences of the generic form (with all coefficients being positive)

$$\begin{aligned} R_{\text{side}}^2(\Phi) &= R_{\text{s},0}^2 + R_{\text{s},2}^2 \cos(2\Phi), & R_{\text{out}}^2(\Phi) &= R_{\text{o},0}^2 - R_{\text{o},2}^2 \cos(2\Phi), \\ R_{\text{os}}^2(\Phi) &= R_{\text{os},2}^2 \sin(2\Phi). \end{aligned} \quad (2)$$

Although the magnitudes of the coefficients R_α^2 in Fig. 6 are quite different (and presumably not too trustworthy, given the disagreement with the data for central collisions in Fig. 3), it is surprising that the signs and phases of the oscillations are identical to those calculated and measured at the AGS [42]! At the AGS radial flow effects are thought to be sufficiently weak that the oscillations can be interpreted purely geometrically [42], reflecting a spatially deformed source which is elongated perpendicular to the reaction plane (as is the case for the initial overlap region). Fig. 5 shows that at RHIC the reason for these oscillations is more subtle: except for small K_\perp , where pions are emitted from the entire fireball, the strong radial flow squeezes the emission regions towards the edge of the fireball so that they no longer reflect directly the spatial deformation of the momentum-integrated emission function shown in Fig. 4. However, even though the measured HBT radii have little to do with the total widths of the fireball in x and y directions, the out-of-plane deformation of the latter imprints itself on the shape of the effective emission regions through the ‘‘opacity

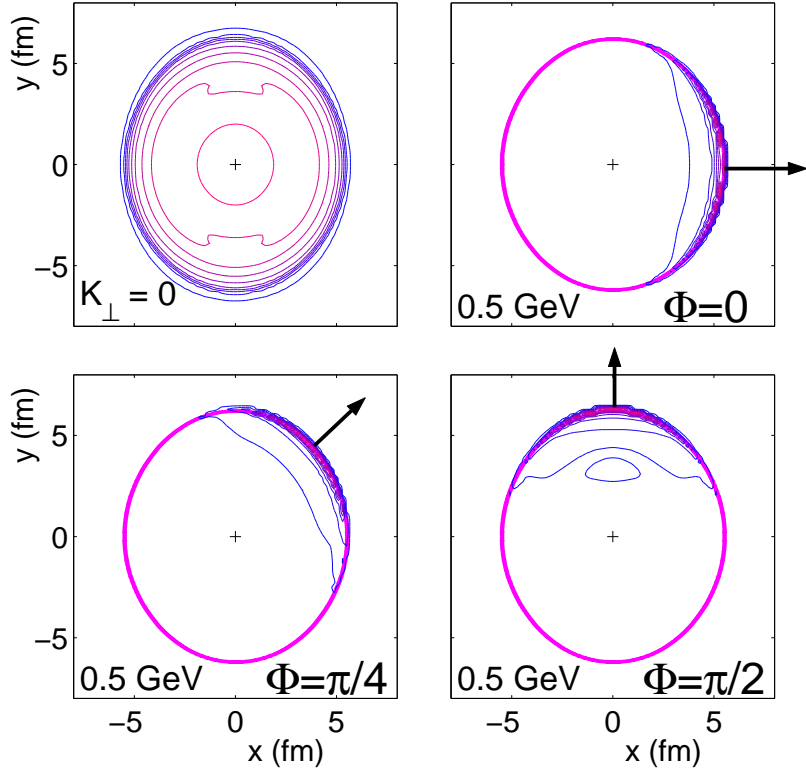


Fig. 5. Time- and z -integrated emission function for $b=7$ fm Au+Au collisions at RHIC for directly emitted pions with rapidity $Y=0$ and fixed transverse momentum K_{\perp} . Shown are contours of constant particle density at freeze-out in the transverse plane, for $K_{\perp}=0$ in the upper left panel, and for $K_{\perp}=0.5$ GeV and three azimuthal emission angles (0° , 45° , and 90° relative to the reaction plane) in the remaining three panels.

effect”, i.e. the fact that the emission is strongly surface-peaked, leading to azimuthal oscillations which are in phase with those expected from naive geometrical considerations of the entire source.

Even though the absolute magnitudes of the radii shown in Fig. 6 are affected by similar problems as those in Fig. 3, the phases of the azimuthal oscillations agree with preliminary STAR data [43], and also their amplitudes are at least in the right ballpark. This gives rise to some optimism that the HBT puzzle is limited in scope and can be resolved by evolutionary rather than revolutionary methods.

Acknowledgement

This work was supported by the U.S. Department of Energy under contract DE-FG02-01ER41190.

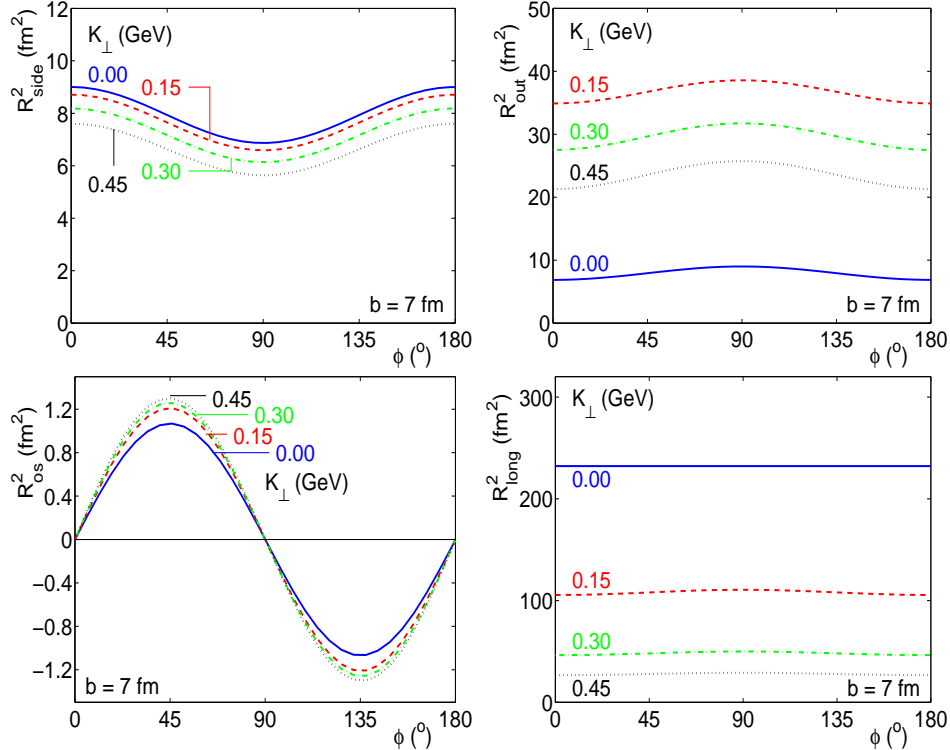


Fig. 6. Azimuthal dependence of the HBT radii from hydrodynamic simulations of RHIC 1 Au+Au collisions at $b = 7 \text{ fm}$, for pion pairs with rapidity $Y = 0$ and various values of K_{\perp} as indicated in the diagrams. The oscillations are about 25% stronger if freeze-out is implemented directly at hadronization (P. Kolb, PhD thesis).

References

1. J.-Y. Ollitrault, *Phys. Rev.* **D46** (1992) 229.
2. S.A. Voloshin and Y. Zhang, *Z. Phys.* **C70** (1996) 665.
3. B. Zhang, M. Gyulassy, and C.M. Ko, *Phys. Lett.* **B455** (1999) 45.
4. D. Molnár and M. Gyulassy, *Nucl. Phys.* **A697** (2002) 495.
5. P.F. Kolb, J. Sollfrank and U. Heinz, *Phys. Rev.* **C62** (2000) 054909.
6. H. Sorge, *Phys. Rev. Lett.* **78** (1997) 2309; *ibid.* **82** (1999) 2048.
7. S.A. Voloshin and A.M. Poskanzer, *Phys. Lett.* **B474** (2000) 27.
8. K.H. Ackermann *et al.* [STAR Collaboration], *Phys. Rev. Lett.* **86** (2001) 402.
9. R.A. Lacey *et al.* [PHENIX Collaboration], *Nucl. Phys.* **A698** (2002) 559c.
10. For a recent compilation of elliptic flow data see A.M. Poskanzer, nucl-ex/0110013.
11. P.F. Kolb, J. Sollfrank, and U. Heinz, *Phys. Lett.* **B459** (1999) 667.
12. D. Teaney, J. Lauret, and E.V. Shuryak, *Phys. Rev. Lett.* **86** (2001) 4783; and nucl-th/0110037.
13. P.F. Kolb *et al.*, *Phys. Lett.* **B500** (2001) 232.
14. P. Huovinen *et al.*, *Phys. Lett.* **B503** (2001) 58.

15. C. Adler *et al.* [STAR Collaboration], *Phys. Rev. Lett.* **87** (2001) 082301.
16. S.C. Johnson [PHENIX Collaboration], *Nucl. Phys.* **A698** (2002) 603c.
17. F. Cooper and G. Frye, *Phys. Rev.* **D10** (1974) 186.
18. S.A. Bass and A. Dumitru, *Phys. Rev.* **C61** (2000) 064909.
19. U. Heinz, *Nucl. Phys.* **A661** (1999) 140c.
20. J.D. Bjorken, *Phys. Rev.* **D27** (1983) 140.
21. P.F. Kolb, U. Heinz, P. Huovinen, K.J. Eskola, and K. Tuominen, *Nucl. Phys.* **A696** (2001) 175.
22. B.B. Back *et al.* [PHOBOS Collaboration], *Phys. Rev. Lett.* **85** (2000) 3100; *Phys. Rev.* **C65** (2002) 031901; and *Phys. Rev. Lett.* **88** (2002) 022302.
23. K. Adcox *et al.* [PHENIX Collaboration], *Phys. Rev. Lett.* **86** (2001) 3500.
24. J. Velkovska *et al.* [PHENIX Collaboration], *Nucl. Phys.* **A698** (2002) 507c.
25. C. Adler *et al.* [STAR Collaboration], *Phys. Rev. Lett.* **87** (2001) 262302.
26. K.S. Lee, U. Heinz, and E. Schnedermann, *Z. Phys.* **C48** (1990) 525.
27. P. Braun-Munzinger *et al.*, *Phys. Lett.* **B518** (2001) 41.
28. R.J. Snellings [STAR Collaboration], *Nucl. Phys.* **A698** (2002) 193c.
29. C. Adler *et al.* [STAR Collaboration], *Phys. Rev. Lett.* **87** (2001) 182301.
30. M. Bleicher and H. Stöcker, *Phys. Lett.* **B526** (2002) 309.
31. Z.W. Lin and C.M. Ko, *Phys. Rev.* **C65** (2002) 034904.
32. U. Heinz and B.V. Jacak, *Ann. Rev. Nucl. Part. Sci.* **49** (1999) 529; U.A. Wiedemann and U. Heinz, *Phys. Rept.* **319** (1999) 145.
33. U. Heinz and P.F. Kolb, hep-ph/0111075.
34. K. Adcox *et al.* [PHENIX Collaboration], nucl-ex/0201008.
35. U.A. Wiedemann and U. Heinz, *Phys. Rev.* **C56** (1997) 3265.
36. B.R. Schlei and N. Xu, *Phys. Rev.* **C54** (1996) 2155; B.R. Schlei, D. Strottman, J.P. Sullivan, and H.W. van Hecke, *Eur. Phys. J.* **C10** (1999) 483.
37. S. Soff, S.A. Bass, and A. Dumitru, *Phys. Rev. Lett.* **86** (2001) 3981.
38. E. Schnedermann and U. Heinz, *Phys. Rev.* **C50** (1994) 1675.
39. P.F. Kolb, M. Tilley, and U. Heinz, in preparation.
40. D.H. Rischke and M. Gyulassy, *Nucl. Phys.* **A608** (1996) 479.
41. B. Tomásik and U. Heinz, nucl-th/9805016; and *Acta Phys. Slov.* **49** (1999) 251 [nucl-th/9901006].
42. M.A. Lisa, U. Heinz, and U.A. Wiedemann, *Phys. Lett.* **B489** (2000) 287; M.A. Lisa *et al.* [E895 Collaboration], *Phys. Lett.* **B496** (2000) 1.
43. F. Retière [STAR Collaboration], nucl-ex/0111013.